14B.2

MECHANISMS OF 20TH AND 21ST CENTURY ASIAN MONSOON CHANGES IN CMIP5 MODELS AND OBSERVATIONS

Xiaoqiong Li *, Mingfang Ting, and Cuihua Li
Lamont-Doherty Earth Observatory, Columbia University, Palisades, New York

1. Introduction

With its large population, increasing industrial development and severe water stresses, Asia is one of the most vulnerable regions in the world facing hydroclimate changes. Piao et al. (2010) assessed the impacts of climate change on water resources and agriculture in China, suggesting a 20% crop production decrease by 2050 under the worst-case scenario. However the overall impact is far from certain due to the high variability and uncertainty in projected climate, particularly precipitation, and the corresponding crop responses. Asian monsoon is one of the major monsoon systems in the world, with critical importance in terms of climate impacts in Asia and globally. Analyzing and understanding the characteristics of monsoon change has important implications for various socioeconomic sectors and human well-being, including water resource management, agriculture, food security, and public health.

There have been extensive observational and modeling studies on Asian monsoon variability, particularly on interannual timescales, revealing strong associations with El Nino Southern Oscillation (e.g., Wang et al. 2000; Kumar et al. 2006; Lau and Nath 2006; Mishra et al. 2012). For the forced change of Asian monsoon, several studies have addressed the weakening monsoon circulation during the second half of the 20th century, both for Indian monsoon (Annamalai et al. 2013) and East Asian monsoon (Song et al. 2013). As for future projections, modeling studies suggest intensification of future monsoon under global warming, both in mean precipitation and extreme events (Ueda et al. 2006; Seo et al. 2013; Wang et al. 2014).

Greenhouse gases and aerosols are the main forces affecting monsoon change. Monsoon rainfall is expected to increase under greenhouse gas induced warming mainly due to more abundant tropospheric water vapor (Ueda et al. 2006). However, sea surface temperature (SST) warming associated with increasing greenhouse gas over the tropical western Pacific could also affect atmospheric circulation and cause a drying trend over South Asia (Annamalai et al. 2013). Considering the severe air pollution problem in Asia in recent years, aerosol effect has become an active topic in Asian monsoon research (e.g., Bollasina et al. 2011; Ganguly et al. 2012; Wu et al. 2013). Increased aerosol concentration in the atmosphere could reduce the surface solar radiation ("dimming" effect), which weakens the SST gradient in the Indian Ocean, reduces local Hadley cell circulation and thereby weakens Indian monsoon (Ramanathan et al. 2005). On the other hand,

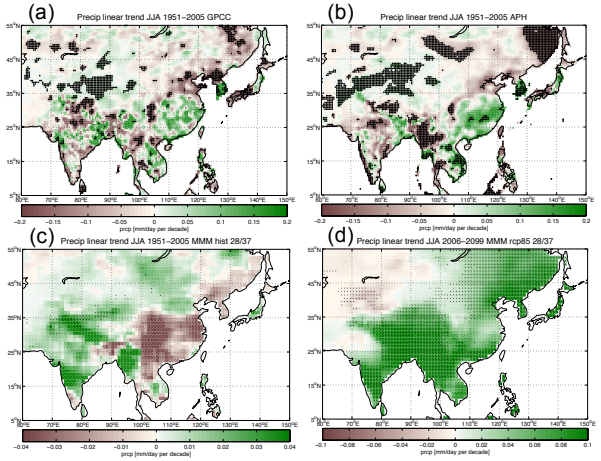

Fig. 1 Linear trends of Jun-Aug precipitation for GPCC 1951-2005 (a), APHRODITE 1951-2005 (b), CMIP5 multi-model mean historical 1951-2005 (c), and rcp8.5 2006-2099 (d) simulations. Units are mm/day per decade. Stippling denotes 5% significance based on 2-sided Student's t-test in (a) and (b) and 28/37 model agreement in (c) and (d).

Lau et al. (2006) have proposed the "elevated heat pump" hypothesis, in which aerosols could enhance the meridional temperature gradient in the mid-to-upper troposphere, causing an advancement and intensification of the Indian summer monsoon rainfall. Thus the question of how Asian monsoon rainfall and circulation may respond to future anthropogenic forcing, including both greenhouse gases and aerosols, is far from conclusive.

Observed linear trends of Asian summer monsoon rainfall (June-August mean from 1951 to 2005) generally shows a slight wetting trend with good agreement between two different datasets (Fig. 1a, GPCC, and Fig. 1b, APHRODITE, details in Section 2), However CMIP5 multi-model simulated pattern over the same time period presents a more dominant drying signal over southeast China and strong wetting over India (Fig. 1c). On the other hand, future projection under the rcp8.5 emission scenario presents a clear wetting trend across the entire monsoon region (Fig. 1d). The discrepancies between observations and model simulations as well as the contrast between past and future changes motivate us to examine further the causal mechanisms and to explore the relative effects of aerosols or greenhouse gases. Given the complex nature of monsoon variability on interannual and decadal timescales, linear trends might not be able to accurately represent anthropogenic changes. Thus it is essential to obtain a better estimate of the forced signal and separate the radiatively forced component for Asian monsoon rainfall from the natural varying component. We use the signal-to-noise maximizing EOF (Ting et al.,

* *Corresponding author address*: Xiaoqiong Li, Lamont-Doherty Earth Observatory, Columbia University, 61 Route 9W, Palisades, NY 10964. E-mail: xqli@ldeo.columbia.edu

2009) technique in this study to obtain a model-based best estimate of the radiatively forced signal in monsoon rainfall.

We examine Asian summer monsoon patterns in response to anthropogenic forcing for June-August seasonal mean using observations and CMIP5 multi-model ensemble historical simulations under all-forcing, greenhouse gas forcing and aerosol forcing scenarios and future projections under rcp8.5 emission scenario. The paper is organized as follows. Section 2 describes observed datasets and model simulations used in the study, as well as the methodology of the analysis. Section 3 presents results regarding past and future changes of Asian summer monsoon, discussions on possible physical mechanisms, and the relative impacts of greenhouse gases and aerosols. The main conclusions are summarized in section 4.

2. Data and Methods

2.1 *Observational and reanalysis data*

We use two gridded observational datasets for precipitation: monthly data from the Global Precipitation Climatology Centre (GPCC) Full Data Product version 5 from the World Climate Research Programme (WCRP) Global Climate Observing System (GCOS) (Schneider et al. 2008), and daily data from Asian Precipitation - Highly-Resolved Observational Data Integration Towards Evaluation (APHRODITE) of the Water Resources project version 1101, created by the Research Institute for Humanity and Nature and Meteorological Research Institute of Japan Meteorological Agency (Yatagai et al. 2012). The spatial resolution is 0.5°×0.5° for both datasets. Observed sea surface temperature is from National Oceanic and Atmospheric Administration (NOAA) National Climate Data Center (NCDC) Extended Reconstructed Sea Surface Temperatures (ERSST), version 3b monthly data, with 2°×2° spatial resolution (Smith et al. 2008). We use 20th Century Reanalysis Project monthly data for wind and specific humidity fields, with 2°×2° spatial resolution.

2.2 *Model simulations*

Model simulations in this study include a multi-model ensemble from World Climate Research Programme (WCRP) Coupled Model Intercomparison Project – Phase 5 (CMIP5) models data output. We use 37 models for historical simulations and future projections under the high-end rcp8.5 emission scenario. All realizations of the models are used, 113 and 77 total runs for historical and rcp8.5, respectively. We also use all available models including all realizations for historical aerosol forcing only (11 models, 37 realizations) and greenhouse gas forcing only (17 models, 49 realizations) experiments. All model outputs have been interpolated to a 1°×1° spatial resolution for precipitation and a 2°×2° spatial resolution for sea surface temperature, wind and moisture fields.

2.3 *Analysis Methods*

We apply signal-to-noise (S/N) maximizing EOF analysis (Allen and Smith 1997) to June-August seasonal average rainfall of the CMIP5 ensemble to extract the externally forced signal, as in Ting et al. (2009). In order to focus on long-term low frequency changes, a Butterworth low-pass filter with 10-year cutoff frequency is applied to monthly data prior to the analysis. Given the multi-model, multi-realization ensemble, the total covariance matrix of the ensemble mean can be assumed as a sum of two linearly independent matrices, one for forced signal and one for internal variability ("climate noise"). The spatial structure of the internal modes of variability is first determined by an EOF analysis on the "noise" matrix, formed using the second century of rainfall anomalies in the preindustrial control run for each of the corresponding model in the analysis. We use 80% of total variance explained to determine the number of noise EOFs entering the pre-whitening process. After applying a spatial pre-whitening transformation to the total covariance matrix to remove these internal varying modes, the spatial covariance in the ensemble average is largely due to forced change. The leading EOF mode of the ensemble mean gives the dominant forced signal. Using the leading principle component (S/N PC1) as the forcing index, we construct the forced patterns of rainfall, circulation and moisture fields using regression analysis. Here the multi-model mean (MMM) is computed as the arithmetic mean of rainfall anomalies across all realizations. We find that using all available realizations has an advantage over using just one realization for each model because it provides a much larger ensemble set to eliminate internal variability. For a multi-model, multi-realization set, there are two common ways of obtaining the MMM: direct averaging across all realizations treating each as equal weight, or, averaging across ensemble members for each model, and then calculate the multi-model mean by averaging over the individual model means. The first method has a certain risk of biasing towards models with more ensemble members, while in the latter, the MMM could easily be affected by models that has only single realization but with larger amplitudes of internal fluctuations. Since the goal of S/N maximizing EOF analysis is detecting long-term forced change through minimizing the effects of natural variability, we find that the first averaging method of using all available realizations proves to be a better way to smooth out internal noise and extract the forced signal. In the regressions, we calculate regression coefficients for each realization and use the second averaging method to obtain the MMM, which allows for the examination of model agreement on the sign of regression coefficients.

3. Results

3.1 *20th and 21st Century forced monsoon changes in observations and CMIP5 models*

The S/N maximizing EOF analysis is performed on 10-year low-pass filtered June to August seasonal mean precipitation over land for the Asian monsoon region (5°N – 55°N, 60°E – 150°E). We use 37 CMIP5 models with 113 and 77 realizations for historical (1861-2005)

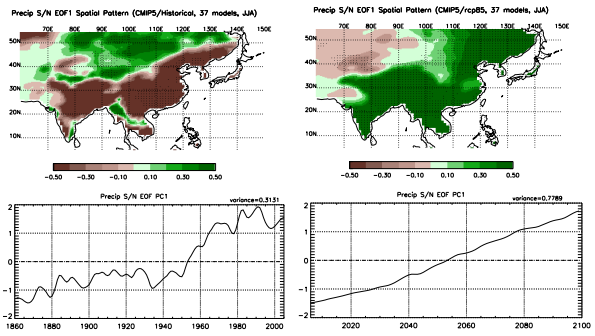

Fig. 2 First modes of S/N maximizing EOF analysis of 10-year Butterworth low-pass filtered Jun-Aug precipitation for historical 1861-2005 (left) and rcp 8.5 2006-2099 (right) simulations using 37 CMIP5 models with 113 (historical) and 77 (rcp8.5) realizations. (top) Spatial structures of the leading modes, shown as MMM of regressions of precipitation onto the S/N PC1. Stippling denotes 28/37 model agreement. (bottom) Standardized S/N maximizing PC1 for MMM.

and rcp8.5 (2006-2099) simulations, respectively. The spatial structures and principle components of the leading S/N modes are given in Figure 2. For the historical period, the dominant signal is a drying trend across South and East Asian monsoon domains, explaining 31% of the total variance. The principle component time series shows there is a sharp increasing trend of the drying signal from the 1940s to 1980s followed by a slight downward trend after the 1980s. For rcp8.5 scenario, there is a clear wetting signal over almost the entire region with an almost linear trend throughout the 21st century. This first mode explains a high percentage (78%) of the total variance, indicating that the externally forced variability of Asian summer monsoon rainfall in the future can be well represented by this uniformly wetting trend.

Figure 3 shows the observed (a) and model simulated (b) Asian summer (Jun-Aug) monsoon rainfall regressed onto PC1 using APHRODITE and CMIP5 historical ensemble, respectively, and CMIP5 rcp8.5 simulations (c). Considering the sparseness of rain gauges and relative low reliability of data prior to 1950, we perform the regressions using 1951-2005 observational data and compare with CMIP5 historical simulations over the same period. Only the results for APHRODITE are shown here given the similarities between GPCC and APHRODITE (Fig.1). For future projections, we use the entire period from 2006 to 2099. While observed pattern associated with S/N PC1 (Fig. 3a) shows no dominant signal with an overall slightly wetting trend, CMIP5 historical MMM (Fig. 3b) indicates a predominantly drying pattern expanding from eastern China to northern India. It is not clear whether this discrepancy between model and observations is due to uncertainty in observations or model deficiencies, although the S/N EOF method does reconcile some of the distinct differences in the linear trend patterns. Neither the significance in observations nor the model agreement in MMM during the historical period is very robust, implying higher level of uncertainty. As for future model projected change under rcp8.5 scenario (Fig. 3c), monsoon rainfall enhances across the entire Asian domain with relatively high model agreement. The associated SST patterns (Fig. 3, d-f), calculated as regressions of global SST onto the forced rainfall indices (S/N PC1) display clear global warming trends in models, but large cooling regions in North Atlantic and North Pacific, in contrasts to strong warming in the other ocean basins in observations. Whether the difference in SST pattern could be the reason for explaining the monsoon rainfall differences between CMIP5 MMM and observations needs to be further examined.

In order to explore the related physical processes, circulation and moisture changes are examined using 850mb winds and specific humidity fields, as shown in Figure 4. CMIP5 models indicate reduced summer monsoon circulation for both Indian and East Asian monsoon in historical simulations (Fig. 4e) while the monsoon circulation intensified in observations (Fig. 4d). In the 21st century rcp8.5 projections (Fig. 4f), Indian monsoon circulation tends to be shifted northward while East Asian monsoon circulation enhances. In all cases, lower troposphere moistens up as the temperature increases (Fig. 4, a-c). Thus the discrepancies in rainfall as seen in Figure 3 are explained by the monsoon circulation changes, rather than the changes in moisture field. In observations, the increase of moisture and intensification of circulation both contribute towards the enhancement of monsoon rainfall. In historical model simulations, the weakened circulation dominates over the increased moisture content, resulting in an overall drying trend. However in the 21st century, increasing water vapor due to greenhouse warming becomes the major force, leading to greatly enhanced summer monsoon rainfall.

3.2 *Impacts of 20th Century aerosol and greenhouse gas forcing*

To examine the relative roles of aerosol and greenhouse gases on monsoon change, we further apply S/N maximizing EOF to June-August rainfall on CMIP5 aerosol-only and greenhouse-only forcing runs during the historical period (1861-2005). We use all realizations of the available CMIP5 models: 11 models with 37 realizations for aerosol forcing and 17 models with 49 realizations for greenhouse forcing. The dominant modes (not shown) exhibit distinctive opposing effects of the two forcings, explaining ~50% of the total variance in both cases (52% for aerosol and 51% for greenhouse). Both the drying signal under aerosol forcing and the wetting signal under greenhouse forcing expand over the entire monsoon region. The PCs display clear upward trends from the 1940s to present.

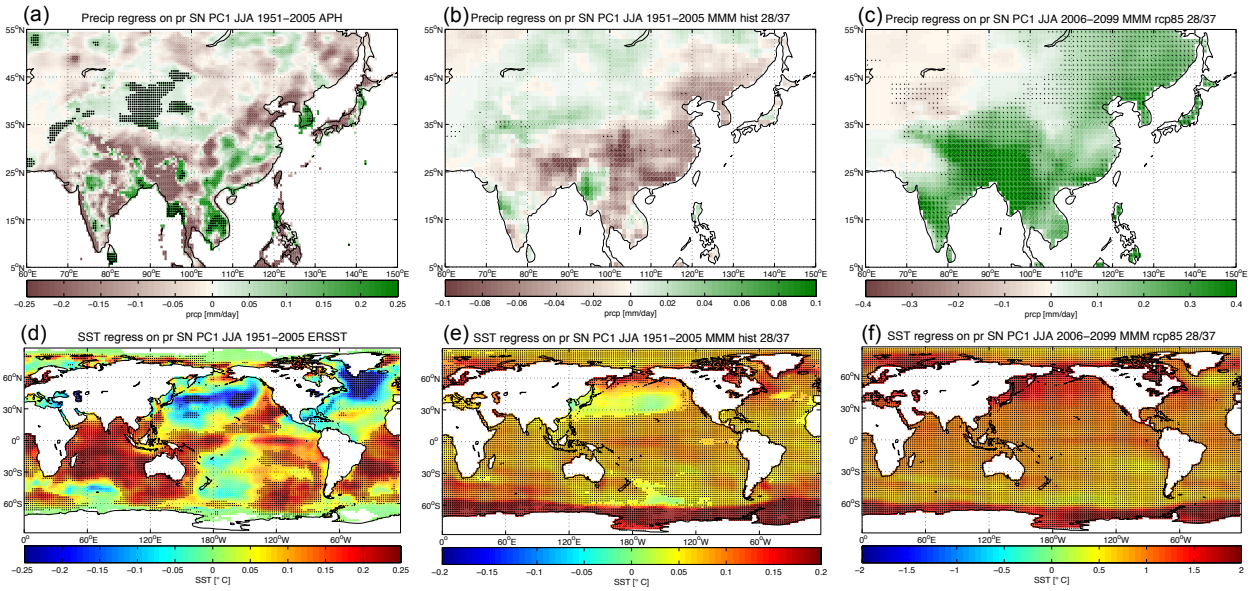

Fig. 3 Regressions of Jun-Aug precipitation (a-c, units are mm/day) and global SST (d-f, units are °C) onto standardized S/N PC1 for observations 1951-2005 (a: APHRODITE; d: ERSST), CMIP5 MMM historical 1951-2005 (b, e), and rcp8.5 2006-2099 (c, f) simulations. Stippling denotes 5% significance based on 2-sided Student's t test in (a, d) and 28/37 model agreement in (b, c, e, f).

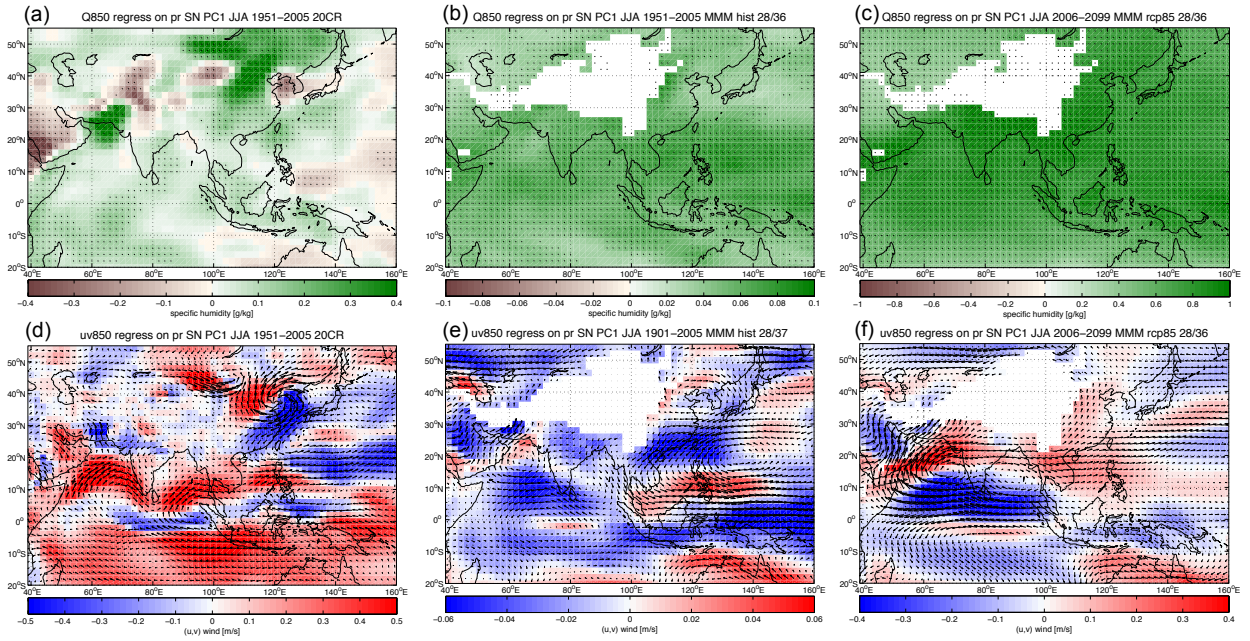

Fig. 4 Regressions of Jun-Aug specific humidity (a-c, units are g/kg) and wind (d-f, units are m/s) at 850mb onto standardized rainfall S/N PC1 for 20th Century Reanalysis 1951-2005(a, d), CMIP5 MMM historical 1951-2005 (b, e), and rcp8.5 2006-2099 (c, f) simulations. In wind plots (d-f), arrows are vectors of regression coefficients of (u, v) wind; colors show the magnitudes of the coefficients. Stippling denotes 5% significance based on 2-sided Student's t test in (a, d) and 28/37 model agreement in (b, c, e, f).

Next we focus on the 20th century (1901-2005) to assess the relative contributions of aerosols and greenhouse gases on the total monsoon change. We standardize the leading PCs from 1901 to 2005 for historical all forcing, aerosol forcing and greenhouse forcing, then perform regression analysis for rainfall (Fig. 5), wind, and moisture fields (Fig. 6). Rainfall reduces under aerosol forcing (Fig. 5b) and increases under greenhouse forcing (Fig. 5c). The total change (Fig. 5a) depends strongly on the relative strengths of these two competing effects. Both aerosol drying and greenhouse wetting effects are strong over central and south India, thus the cancelations lead to a mixed pattern. Over east China and northeast India, however, the aerosol forcing tends to dominate over the greenhouse effect, resulting in strong drying trends. Considering that these regions

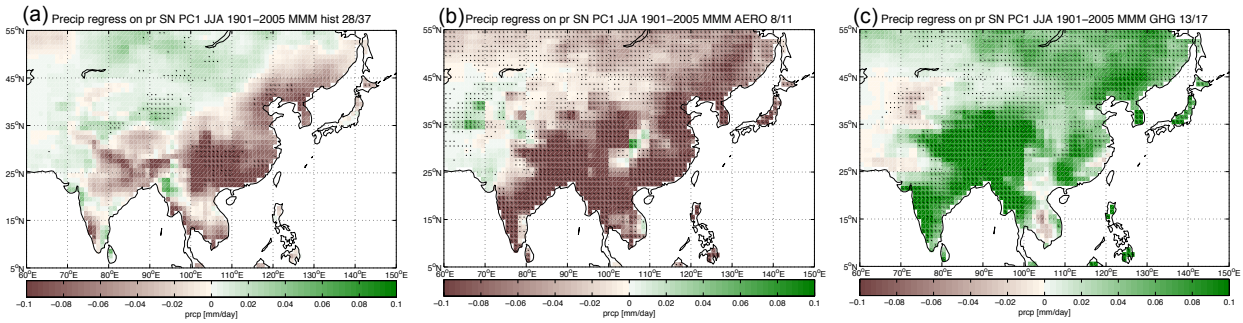

Fig. 5 Regressions of Jun-Aug precipitation (mm/day) onto standardized rainfall S/N PC1 from 1901 to 2005 for CMIP5 multi-model historical all forcing (a), aerosol forcing (b), and greenhouse gas forcing (c) simulations. Stippling denotes model agreement of 28/37, 8/11 and 13/17 for (a), (b) and (c), respectively.

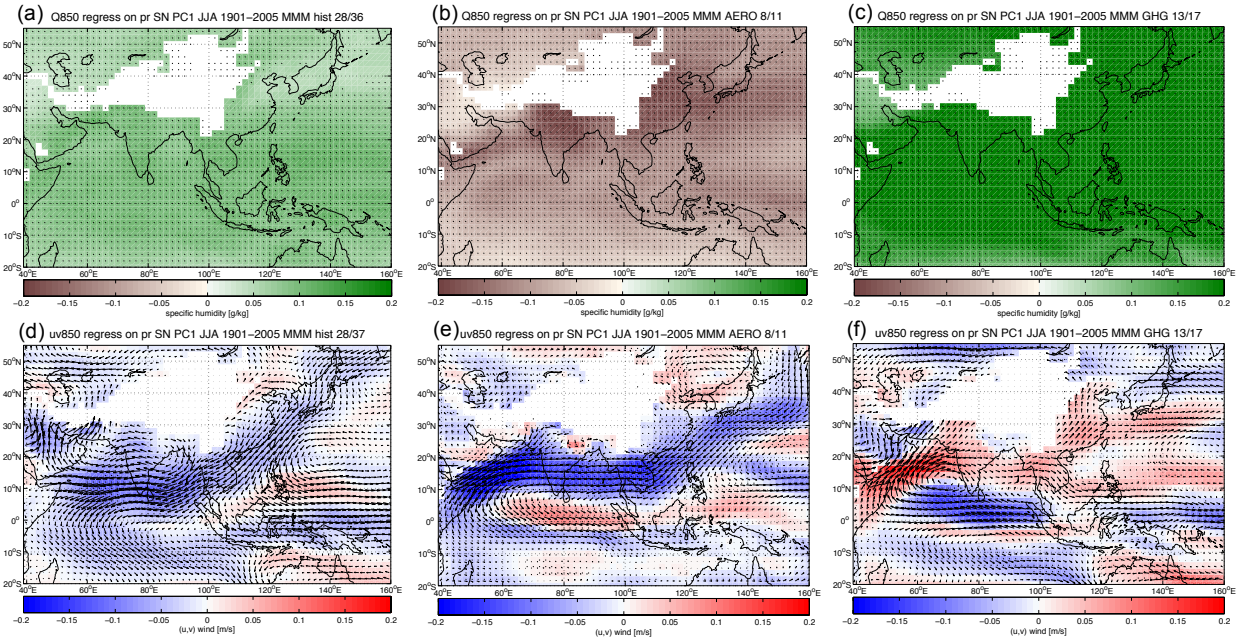

Fig. 6 Regressions of Jun-Aug specific humidity (a-c, units are g/kg) and wind (d-f, units are m/s) at 850mb onto standardized rainfall S/N PC1 for CMIP5 multi-model all forcing (a, d), aerosol forcing (b, e), and greenhouse gas forcing (c, f) simulations. In wind plots (d-f), arrows are vectors of regression coefficients of (u, v) wind; colors show the magnitudes of the coefficients. Stippling denotes model agreement of 28/37, 8/11 and 13/17 for (a, d), (b, e) and (c, f), respectively.

also display the largest discrepancies between observed and modeled changes, the results here imply that these discrepancies might be caused by the overestimation of aerosol effect in CMIP5 model simulations. For SST, lower tropospheric water vapor reduces under aerosol effect (Fig. 6b) while enhancing greatly under greenhouse warming (Fig. 6c). The warming effect plays the dominant role that contributes to the overall enhancement under all-forcing scenario with weaker amplitudes (Fig. 6a). For wind field, aerosols weaken low-level monsoon circulation (Fig. 6e) while greenhouse effect shifts Indian monsoon circulation northward and enhances East Asian monsoon circulation (Fig. 6f). In this case, aerosol effect has the dominant role, resulting in weakened total monsoon circulation (Fig. 6d). Overall, the weakening of the monsoon circulation due to aerosol appears to be the dominant factor to the drying trend in CMIP5 historical simulations. Also note that the greenhouse forcing patterns are very similar to those under rcp8.5 scenario, confirming the dominant role of increasing moisture content in the greenhouse future.

The roles of aerosol and greenhouse gas forcing are further examined by taking the differences between historical and greenhouse-only and historical and aerosol-only for the late 20th Century (1971-2005) to represent the effect of aerosol and greenhouse gas forcing, respectively. The resulting monsoon rainfall and circulation differences (not shown) are very similar to that in Figs. 5 and 6, confirming the robustness of the S/N EOF method for estimating the forced signals.

4. Summary

Using S/N maximizing EOF analysis on the CMIP5 multi-model, multi-realization ensemble, we have

extracted a model-based best estimate of the externally forced signal for Asian summer monsoon rainfall. The 20th and 21st Century changes of Asian summer monsoon in response to anthropogenic forcing are examined using both observational data and CMIP5 model simulations. Results show that in the second half of the 20th century, CMIP5 models indicate a predominantly drying pattern expanding from eastern China to northern India. However there are significant discrepancies when compared to observed pattern, which indicates an overall slight wetting trend. For 21st century under rcp8.5 scenario, monsoon rainfall enhances across the entire Asian domain. Projecting low-level moisture and wind fields onto the rainfall forced index show that in historical model simulations, the weakened circulation dominates over the increased moisture content, resulting in an overall drying trend. However in the 21st century, greatly increasing water vapor due to greenhouse warming leads to enhanced summer monsoon rainfall. We have further assessed the relative contributions of aerosols and greenhouse gases on the overall 20th century monsoon change. Rainfall reduces under aerosol forcing and increases under greenhouse forcing, thus the total change depends strongly on the relative strengths of these two competing effects. For 20th century, reduced monsoon circulation driven by aerosol forcing appears to be the dominant contribution to the drying trend in CMIP5 model simulations. The results also imply that the discrepancies between observations and modeled patterns might be caused by the overestimation of aerosol effect in model simulations. Further analysis is needed to obtain a better understanding of the physical mechanisms for the changes and how to reconcile the modeled results with the observed changes during the historical period.

Acknowledgements. This research was supported by NOAA Award NA10OAR4310137 (Global Decadal Hydroclimate Variability and Change).

References

Allen, M. R., and L. A. Smith, 1997: Optimal filtering in singular spectrum analysis. *Phys. Lett.*, **234**, 419–428.

Annamalai H., Jan Hafner, K. P. Sooraj, and P. Pillai, 2013: Global warming shifts the monsoon circulation, drying South Asia. *J. Climate*, **26**, 2701–2718.

Bollasina M. A., Y. Ming and V. Ramaswamy, 2011: Anthropogenic aerosols and the weakening of the South Asian summer monsoon. *Science,* **334**, 502.

Ganguly D., P. J. Rasch, H. Wang, and J. Yoon, 2012: Fast and slow responses of the South Asian monsoon system to anthropogenic aerosols. *Geophys. Res. Lett.*, **39**, L18804.

Krishna Kumar K., B. Rajagopalan, M. Hoerling, G. Bates, and M. Cane, 2006: Unraveling the mystery of Indian monsoon failure during El Niño. *Science,* **314**, 115.

Lau K. -M., M. K. Kim, and K. -M. Kim, 2006: Aerosol induced anomalies in the Asian summer monsoon: The role of the Tibetan Plateau, *Clim. Dyn.,* **26**, 855–864.

Lau N. -C. and M. J. Nath, 2006: ENSO modulation of the interannual and intraseasonal variability of the East Asian monsoon - A model study. *J. Climate*, **19**, 4508–4530.

Mishra V., B. V. Smoliak, D. P. Lettermaier and J. M. Wallace, 2012: A prominent pattern of year-to-year variability in Indian summer monsoon rainfall. *Proc. Natl. Acad. Sci.,* **109**(19), 7213-7217.

Piao S. et al., 2010: The impacts of climate change on water resources and agriculture in China. *Nature,* **467**, 43–51.

Ramanathan V. et al. 2005: Atmospheric brown clouds: Impacts on South Asian climate and hydrological cycle. *Proc. Natl. Acad. Sci.,* **102**(15), 5326-5333.

Schneider U., T. Fuchs, A. Meyer-Christoffer, and B. Rudolf, 2008: Global precipitation analysis products of the GPCC. Global Precipitation Climatology Centre (GPCC), DWD, Internet publication: 1-12.

Seo K., J. Ok, J. Son, and D. Cha, 2013: Assessing future changes in the East Asian summer monsoon using CMIP5 coupled models. *J. Climate*, **26**, 7662–7675.

Song F, T. Zhou, and Y. Qian, 2013: Responses of East Asian summer monsoon to natural and anthropogenic forcings in the 17 latest CMIP5 models. *Geophys. Res. Lett.,* doi: 10.1002/2013GL058705.

The Twentieth Century Reanalysis Project Version 2. Data provided by the NOAA/OAR/ESRL PSD, Boulder, Colorado, USA, from their Website at http://www.esrl.noaa.gov/psd/.

Ting M., Y. Kushnir, R. Seager, and C. Li, 2009: Forced and internal twentieth-century SST trends in the North Atlantic. *J. Climate,* **22**(6), 1469–1481.

Ueda H., A. Iwai, K. Kuwako, and M. E. Hori, 2006: Impact of anthropogenic forcing on the Asian summer monsoon as simulated by eight GCMs. *Geophys. Res. Lett.*, **33**, L06703.

Wang B., S. -Y. Yim, J -Y. Lee, J. Liu, and K. -J. Ha, 2014: Future change of Asian-Australian monsoon under RCP 4.5 anthropogenic warming scenario. *Clim. Dyn.,* **42** (1-2), 83-100.

Wang B., R. Wu and X. Fu, 2000: Pacific-East Asian teleconnection: How does ENSO affect East Asian climate? *J. Climate,* **13**, 1517-1536.

Wu L., H. Su, and J. H. Jiang, 2013: Regional simulation of aerosol impacts on precipitation during the East Asian summer monsoon. *J. Geophys. Res. Atmos.*, **118**, 6454–6467.

Yatagai, A., K. Kamiguchi, O. Arakawa, A. Hamada, N. Yasutomi, and A. Kitoh, 2012: APHRODITE: Constructing a Long-Term Daily Gridded Precipitation Dataset for Asia Based on a Dense Network of Rain Gauges. *Bull. Amer. Meteor. Soc.*, **93**, 1401–1415.